Nucleation and growth of single layer graphene on electrodeposited Cu by cold wall CVD

Shantanu Das[#] *and Jeff Drucker**[,$]

[#]Department of Materials Science and Engineering, School for Engineering of Matter Transport and Energy, Arizona State University, Tempe, Arizona 85287-6106, USA

[$] Department of Physics, Arizona State University, Tempe, Arizona 85287-1504, USA

ABSTRACT

The nucleation density and average size of graphene crystallites grown using cold wall chemical vapor deposition (CVD) on 4μm-thick Cu films electrodeposited on W substrates can be tuned by varying growth parameters. Growth at a fixed substrate temperature of 1000°C and total pressure of 700 Torr using Ar, H_2 and CH_4 mixtures enabled the contribution of total flow rate, CH_4:H_2 ratio and dilution of the CH_4/H_2 mixture by Ar to be identified. The largest variation in nucleation density was obtained by varying the CH_4:H_2 ratio. The observed morphological changes are analogous to those that would be expected if the deposition rate were varied at fixed substrate temperature for physical deposition using thermal evaporation. The graphene crystallite boundary morphology progresses from irregular/jagged through convex hexagonal to regular hexagonal as the effective C deposition rate decreases. This observation suggests that edge diffusion of C atoms along the crystallite boundaries, in addition to H_2 etching, may contribute to shape evolution of the graphene crystallites. These results demonstrate that graphene grown using cold wall CVD follows a nucleation and growth mechanism similar to hot wall CVD. As a consequence, the vast knowledge base relevant to hot wall CVD may be exploited for graphene synthesis by the industrially preferable cold wall method.

1. INTRODUCTION

Graphene is a promising material for many applications that can be exfoliated from bulk graphite or grown using a variety of vapor deposition processes. [1-4] Perhaps the most widely employed method for growth of single-layer graphene is hot-wall chemical vapor deposition (CVD) from gaseous hydrocarbons onto catalytic metal substrates. [5-12] Cu foil has become the most popular of the metal substrates. By virtue of the very low bulk solubility of C, graphene CVD onto Cu is almost entirely a surface mediated process. [11-13] A wide range of CVD process parameters have been employed to grow graphene from a variety of C-containing precursors and gaseous ambients. [14-20] Many investigations have employed methane (CH_4) and hydrogen (H_2) as the active gases and argon (Ar) as the carrier/diluent. [16-20] The majority of investigations into graphene synthesis have focused on empirically reducing the graphene nucleation density to achieve large single-crystal graphene domains to enable large-scale device integration or other applications. [21-24]

Cold wall CVD offers distinct advantages over hot wall CVD. These advantages, which have led to wide acceptance of the technique in microelectronics manufacturing, include a significant reduction

in gas phase chemical reactions and rapid sample heating and cooling that can significantly reduce growth times. Despite these advantages, cold wall CVD is rarely used to grow graphene. Consequently, the relationship between growth parameters and film morphology is not well understood. Existing reports have focused on fabrication of continuous single-layer films or on optimizing growth parameters to produce large single crystal nuclei. These efforts have employed low pressure CVD (LPCVD) at total pressures in the 10s of millitorr to few Torr range. [4, 25, 26] They find that graphene grown using cold wall CVD can progress by either of two very different growth modes. The first is similar to that observed for hot wall CVD; formation of isolated nuclei that impinge to form a continuous film. [4, 26, 27] In contrast, Bointon, et al., [25] suggest that the graphene film evolves from a thick carbon layer formed at early growth stages. They find that this thick layer becomes thinner and forms isolated nuclei that finally impinge to form a complete film.

Even for hot wall CVD, relatively few efforts have systematically varied CVD process parameters in order to quantify their effects on graphene film morphology. Those that have primarily investigated the effect of substrate temperature on graphene film morphology. Vlassiouk, *et al*., varied the growth temperature during hot wall atmospheric pressure CVD (APCVD) and low-pressure LPCVD of graphene onto Cu foils to extract the activation energy for graphene nucleation. [28] They also demonstrated the value of growth at high background pressures for suppressing Cu sublimation during growth near the melting point of Cu. In a similar study, Xing, *et al*., employed hot wall APCVD to investigate temperature effects on the growth of single, bi- and few layer graphene films. [29]

Graphene growth via metal catalyzed decomposition of gaseous hydrocarbons proceeds by a complex sequence of steps, each with its own thermally activated rate. Due to this complexity, achieving fundamental insight into the mechanisms responsible for the observed morphology variation as a function of growth temperature is challenging. For this reason, we investigate graphene grown on Cu at a fixed substrate temperature of 1000°C while systematically varying the composition and total flow rate of the gas phase precursors. In this manner, we identify effects related to the precursor composition and flow on graphene growth. We also grow at fixed total pressure of 700 Torr so that effects related to Cu sublimation are nearly the same for each sample [28,30]. We employ cold wall CVD in a vertical flow configuration from mixtures of Ar, H_2 and CH_4 onto 4 μm-thick Cu films electrodeposited onto W supports. We find that, for the range of growth parameters investigated, greater variation of graphene nucleation density is attained by varying the H_2:CH_4 ratio than by fixing the H_2:CH_4 ratio and diluting this mixture with Ar. We achieved the smallest variation in graphene nucleation density by varying the total precursor flow rate.

We also correlate the shape of isolated graphene nuclei with growth parameters. We find that at the highest effective C deposition rates, some of the crystallites are bound by jagged, irregular edges. At lower deposition rates, the nuclei assume a convex hexagonal morphology. Finally, at the lowest deposition rates, the crystallites are regular hexagons. Similar shapes were observed by Vlassiouk, et al., who suggested that a balance between H etching and C incorporation led to jagged boundaries and argued that more rapid C incorporation at the vertices of hexagonal nuclei produced the convex boundaries. [28] We suggest that while these effects may be important, the relative rates of C incorporation and diffusion along the edges of graphene nuclei likely also play important roles in shape selection during growth.

Our systematic characterization of film morphology as a function of growth parameters conclusively determines that graphene grown using cold wall CVD follows a nucleation and growth mechanism. We find that isolated graphene crystallites nucleate at random locations on the bare Cu substrate. Existing crystallites grow as additional nucleation occurs until a saturation nucleation density is reached. Further deposition enables these crystallites to continue growing until they impinge to form a polycrystalline graphene layer. These results indicate that much of the considerable knowledge base pertaining to graphene synthesis using hot wall CVD may be relevant for the industrially preferred cold wall CVD method.

2. EXPERIMENTAL METHODS

Graphene synthesis was carried out in a home-built multi-chamber cold wall chemical vapor deposition system. The system comprises a load lock for quick sample exchange, an ion pumped buffer chamber, and a CVD chamber for graphene growth on supported thin metal films. In the CVD chamber, we employed a vertical flow configuration with the precursor gas flow directed normal to the substrate surface. Samples can be transferred through the buffer chamber into the growth chamber after the load lock has been turbo pumped to the 10^{-7} Torr range, which required about 30 minutes. During transfer, the buffer chamber pressure rose to 10^{-8} Torr and recovered to its base pressure of $7x10^{-10}$ Torr in about 1 hour. The base pressure of CVD chamber is in the low 10^{-9} Torr range. The buffer chamber is isolated from the load lock and the CVD chamber by gate valves. The graphene CVD chamber is schematically depicted as supplementary figure S1.

During graphene growth in the CVD chamber, sample temperature, total pressure and precursor flow were computer-controlled via a LabVIEW interface ensuring precise run-to-run repeatability. Sample temperature was monitored using an Omega IR 2C infrared pyrometer with an accuracy of ±10 °C. Ultra-high purity Ar, CH_4 and H_2 flow rates were regulated by individual mass-flow controllers and the chamber pressure was monitored using a capacitance manometer. The pressure was regulated via the LabVIEW interface using a down-stream throttle valve. The CVD chamber is pumped by a 210 L/s turbomolecular pump (TMP) backed by a rotary vane mechanical pump. For graphene growth at total gas flow rates greater than 150 sccm (a flow of 1 cm^3/min at standard temperature and pressure), the TMP was switched off.

A typical growth began with preparation of the refractory metal supports. 125 μm thick 99.95% pure W foil was cut into 30 mm x 2mm strips. These strips were then annealed at 2000°C in batches of 20 in an Ar ambient at atmospheric pressure for 6 hours to reduce surface roughness and increase the polycrystalline grain size. After the strips were annealed, any native oxide was removed by dipping in a freshly prepared 2 molar solution of KOH/water. The strips were subsequently sonicated in first acetone and then methanol.

Graphene was grown on 4 μm-thick Cu films electrodeposited on the annealed W supports. Cu was deposited from an electrolyte solution of 1M $CuSO_4$ and 1M H_2SO_4 using a 6N Cu foil counter electrode at a current of 5 mA for 85 min. After electrodepositing the Cu film, the Cu/W substrate was rinsed in deionized water and sonicated in methanol. The freshly-prepared substrates were then secured to the sample holder by Ta electrodes and loaded in the load lock. After pumping to high vacuum, the electrodeposited substrates were transferred directly to the CVD chamber.

Our CVD system is capable of graphene synthesis over a wide range of total gas pressures using a wide range of Ar, H_2 and CH_4 flow rates. Ar:H_2:CH_4 ratios were controlled by varying the flow rates of the individual gases over the following ranges; CH_4: 0.25-5 sccm; H_2: 50-1000 sccm and

Ar: 500-10,000 sccm. Total pressure during growth can be varied in the range 10^{-3} to 700 Torr, but the graphene films discussed here were all prepared at a pressure of 700 Torr. Graphene was grown using cold wall CVD onto substrates that were resistively heated using direct current to 1000°C.

After transfer to the CVD chamber, the Cu/W substrate was annealed at 1000°C in a reducing atmosphere of Ar and H_2 at a total pressure of 700 Torr for 15 minutes. The Ar and H_2 flow rates were identical to those employed for subsequent graphene growth. The average grain size of the Cu film after annealing was ~60 micrometers, up from about 5 μm for the unannealed films. Immediately following this annealing step, CH_4 was supplied to initiate graphene growth. By employing total gas flow rates near 10,000 sccm for most growths, we ensured that steady state growth conditions were reached in a time that was small compared to the graphene growth time. The volume of the CVD chamber is ~7 liters and at flow of about 10000 sccm the entire volume of the chamber is exchanged in less than 40 seconds. In this manner, we can define an accurate graphene nucleation time, which is the time after CH_4 flow was initiated required for the first graphene crystallites to nucleate. As discussed in further detail below, we find that growth at lower flow rates requires greater time to reach a particular graphene coverage and results in a lower density of larger graphene crystallites.

After the desired growth time, we simultaneously terminated the CH_4 flow and reduced the substrate heating current to stop graphene growth. While we can reduce the temperature of our resistively heated samples to <450ºC in ~3 sec, the substrate temperature was instantaneously reduced to 900°C when the CH_4 flow was terminated and then in steps of 100°C/min. Our capability for rapidly reducing the growth temperature, in combination with our use of cold wall CVD enables us to precisely delineate the end of graphene growth. After terminating graphene growth, the Ar and H_2 MFCs were closed, the throttle valve was opened and the chamber was pumped to its base pressure. The sample was then allowed to cool down for at least 30 minutes prior to removal for *ex situ* characterization.

Graphene film morphology was characterized using field-emission scanning electron microscopy (FESEM). A Hitachi S4700 FESEM operating at 5 keV was used to obtain ~few nm spatial resolution images of the graphene domains directly on the Cu surface without any *ex situ* processing of the as-grown films. The digitally acquired images were analyzed using ImageJ [31] to quantify the size and nucleation density of the graphene domains.

We also characterized the graphene layer directly on the Cu surface using Raman spectroscopy. The micro-Raman data was acquired in the back scattering geometry. The Raman spectra were excited with a He-Cd laser operating at 442 nm (2.805 eV) which resulted in reduced fluorescence from copper. Using a 0.8 NA objective, an approximately 1μm diameter focus was obtained at the sample. Scattered light was collected, polarized and energy dispersed through a 0.5 m Acton spectrometer and detected with 3 cm^{-1} FWHM (full width at half maximum) resolution using a Princeton Instruments back-thinned Si CCD camera. All graphene films discussed below were comprised of single-layer domains as evidenced by the typical characteristics observed for Raman spectra of monolayer graphene. Namely, a G peak at ~1580 cm^{-1}, a symmetric 2D peak at ~2690 cm^{-1} with a FWHM of ~40 cm^{-1} and a large I(2D)/I(G) ratio (~4.2) of the intensities of the 2D and G peaks. [32-35] A defect peak at 1355 cm^{-1} was also observed. The Raman spectrum is shown in supplementary figure S2.

3. RESULTS AND DISCUSSION

Figure 1 shows a SEM image of typical single-layer hexagonal graphene crystallites grown using cold wall ambient pressure CVD onto electrodeposited Cu. This sample was grown at a pressure of 700 Torr, substrate temperature of 1000ºC, CH_4, H_2 and Ar flow rates of 0.7, 280 and 10,000 sccm, respectively for 42.5 minutes. The graphene crystallites are evident as the dark hexagonal features on the lighter Cu film. Polycrystalline Cu grains in are delineated by the white irregular grain boundaries. Within some of the grains are rectangular bands of different contrast. These are annealing twins that can form when Cu films are annealed at high temperature. The graphene crystallites appear to nucleate at random locations on the Cu film and do not correlate with grain boundaries or annealing twins.

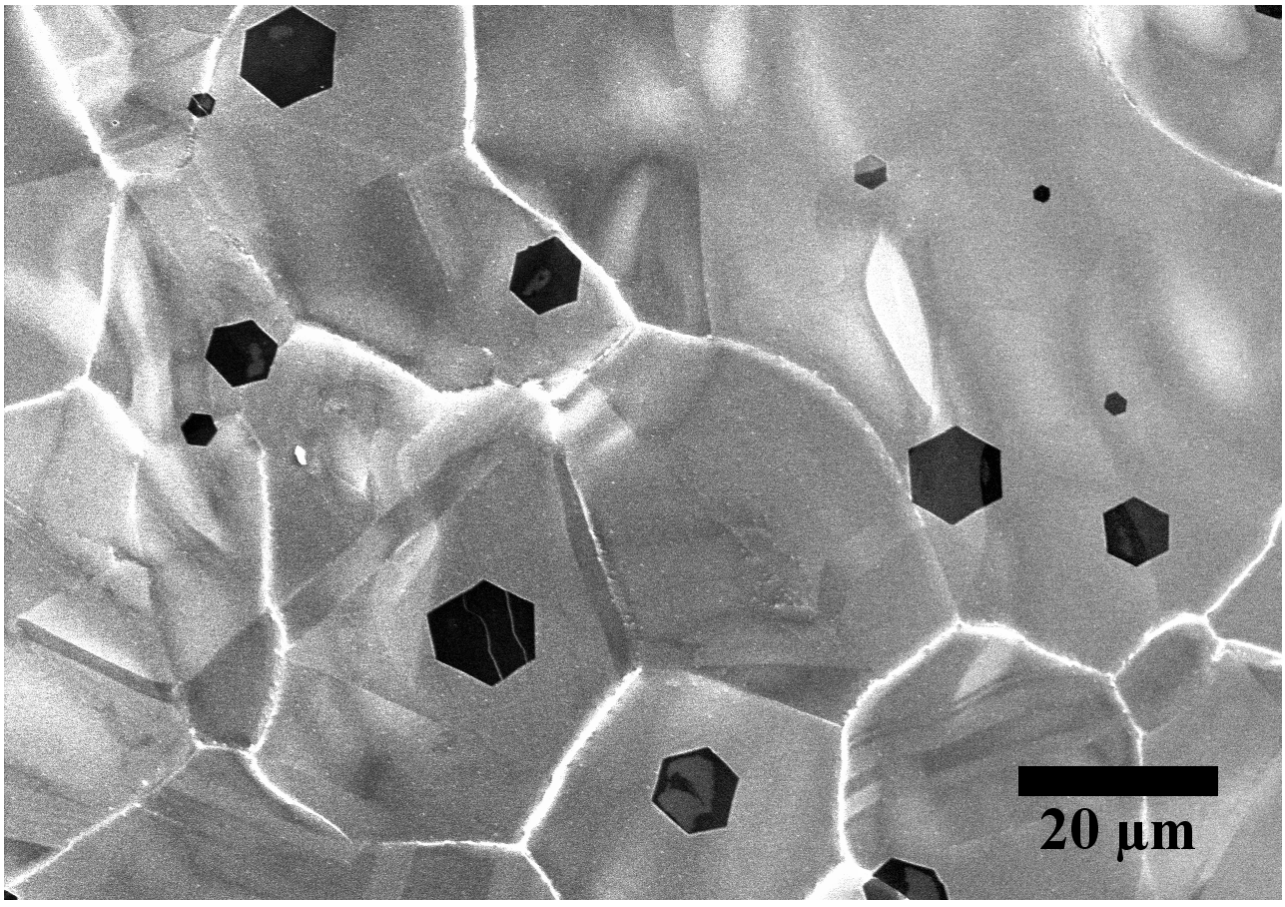

Figure 1. SEM image of graphene crystallites grown on a 4 μm-thick Cu film electrodeposited on 125 μm-thick W. The graphene was grown at 700 Torr and a substrate temperature of 1000 °C using 10,000, 280 and 0.7 sccm flows of Ar, H_2 and CH_4, respectively for 42.5 minutes.

To characterize the effects of different growth conditions on graphene film morphology we performed three series of growths. In the first series, we explored graphene growth at the same CH_4 : H_2 ratio using different dilutions with Ar. The second series investigated graphene film morphology for growth at different CH_4 : H_2 ratios. Both of the first two growth series employed Ar flows of 10,000 sccm. The final series explored the effects of growth at different total flow rates using identical CH_4 : H_2 : Ar flow ratios.

Fixed CH_4:H_2 = 1 : 200 at different Ar dilutions

For this growth series, we fixed the CH_4:H_2 ratio at 1:200 and the Ar flow rate at 10,000 sccm. Three different Ar dilutions were investigated corresponding to CH_4:H_2 flow rates (measured in sccm) of 0.7:140, 2.5:500 and 5:1000. All growths employed a substrate temperature of 1000ºC and pressure of 700 Torr. As discussed below, we varied the growth time for each of these growth conditions to access the different regimes of film growth: nucleation, growth and impingement and coalescence.

Figure 2(a) plots the average size and nucleation density of graphene crystallites vs. growth time, t, for each of the three growth conditions. We employ the diameter of a circle with the same area of a graphene nucleus as a convenient measure of its size. The grains of our polycrystalline Cu films almost certainly have different crystallographic orientations and it is believed that the graphene nucleation density may vary with Cu grain orientation. [28, 36] However, the substrate area analyzed to produce the areal density plotted in figure 2(a) was at least 10^5 μm^2, which contains a large enough number of grains so that grain-to-grain variations were averaged out. Supplementary figure S3 shows a typical set of scanning electron micrographs that were analyzed to produce the data presented below in figures 2-6.

The nucleation density plots in figure 2(a) can be demarcated into regions suggesting that graphene grown by cold wall APCVD on electrodeposited Cu films proceeds by a classical nucleation and growth mechanism. The initial time period for which graphene nuclei have not yet formed (e.g., t < 20 min for the 0.7:140 plot) indicates C undersaturation on the Cu surface. During this time period, the chemical potential of diffusing C-containing species is too low to drive nucleation of stable graphene clusters. Stable graphene clusters form only when the C chemical potential rises high enough to drive nucleation. Subsequent to nucleation of the first graphene crystallites, additional nucleation occurs and the nucleation density increases in conjunction with growth of existing nuclei. This behavior characterizes the nucleation regime and is observed in the 0.7:140 plot during 20 < t < 25 min. Despite continued C deposition as a result CH_4 decomposition, nucleation ceases when all additional C can diffuse to existing graphene nuclei. In this situation, the C chemical potential stabilizes at a level below that required for continued nucleation and the saturation nucleation density, N_{sat}, is reached. For the 0.7:140 series of growths, N_{sat} is near 1.5 x 10^5 cm^{-2} and is evident as the plateau in the nucleation density plot for t > 25 min. Once the saturation nucleation density is reached, continued deposition results in growth of existing graphene nuclei during the growth regime. Similar nucleation and growth regimes can also be identified for the 5:1000 and 2.5:500 plots. Ultimately, the graphene nuclei grow to a size at which they impinge to eventually form a continuous, usually polycrystalline graphene layer. At the onset of graphene grain impingement, tracking the size of individual graphene nuclei becomes challenging.

Figure 2(b) summarizes the results of figure 2(a) by plotting the saturation nucleation density and the average graphene nucleus size at the time N_{sat} is reached. We also plot $N_{sat}^{-1/2}$, which is a useful measure of the average graphene grain size in a completed, presumably polycrystalline single-layer film. It is evident that as the Ar dilution decreases at fixed CH_4 : H_2, the average size decreases and N_{sat} increases. Similar behavior would be expected for growth via physical vapor deposition using thermal evaporation (PVD) for which the substrate temperature was fixed but the deposition rate was increased. PVD by thermal evaporation is conceptually simpler than CVD due to the absence of chemical processes. For graphene growth considered here, these chemical processes include CH_4 decomposition, the interaction between CH_4 and H_2 and H_2 etching. In a PVD process, atoms deposit on and diffuse along the substrate surface and either desorb or incorporate into the growing film. As a consequence, in the absence of desorption, the saturation nucleation density is simply related to the D/F ratio (D is the diffusion constant and F is the deposition flux).[37, 38] D depends only on the substrate temperature for a given material system and all results reported here are for a fixed substrate temperature of 1000°C. Consequently, we can gain further insight into the observed growth dynamics by simplifying interpretation of our results in analogy to a PVD process. In this case, the relevant deposition parameter is the C deposition rate.

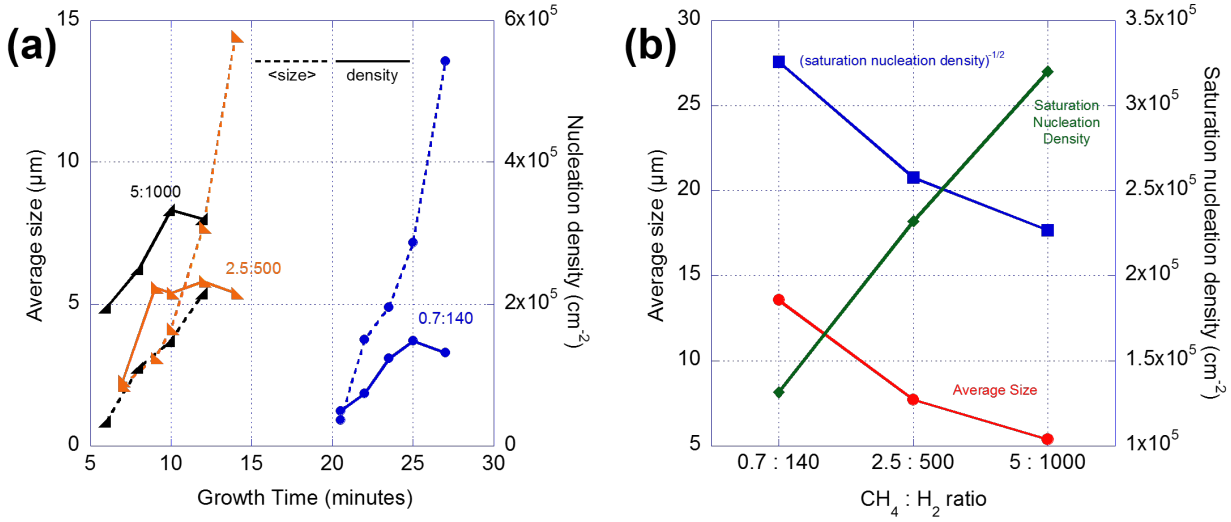

Figure 2. (a) plots the average size and nucleation density of graphene crystallites vs. growth time, t. The samples were grown at the indicated CH_4 : H_2 flow rates (in sccm) using an Ar flow rate of 10,000 sccm, a total pressure of 700 Torr and a substrate temperature of 1000 °C. Each nucleation density plot shows a nucleation regime for which a continuous increase is observed; *e.g.*, from 20 to 25 min for the 0.7:140 plot. Upon reaching the saturation nucleation density, N_{sat}, the average size continues to increase during the growth regime. The growth regime is evident as the plateau at t > 25 min in the 0.7:140 plot. (b) summarizes the results plotted in (a) plotting N_{sat} and the average size at the time N_{sat} is reached vs. CH_4 : H_2 ratio. Also plotted is $N_{sat}^{-1/2}$, which measures the average grain size in a complete single-layer graphene film. The behavior depicted suggests that graphene grows via a conventional nucleation and growth mechanism and that diluting identical CH_4:H_2 ratios is analogous to varying the deposition rate in a PVD process.

For PVD, as the deposition rate is increased at fixed substrate temperature, the average cluster size decreases and the saturation nucleation density increases. Although varying the partial pressure of gaseous precursors in a CVD process may affect reaction kinetics in a complex manner, the behavior depicted in figure 2(b) suggests that diluting a fixed CH_4:H_2 mixture with inert Ar is analogous to varying the deposition rate in a physical vapor deposition process using thermal evaporation. As the fixed composition CH_4/H_2 mixture is diluted, their partial pressures vary in the same ratio as does the rate at which they impinge on the substrate. As a consequence, the rate of CH_4 decomposition and subsequent formation of diffusing C-containing species on the Cu substrate also varies.

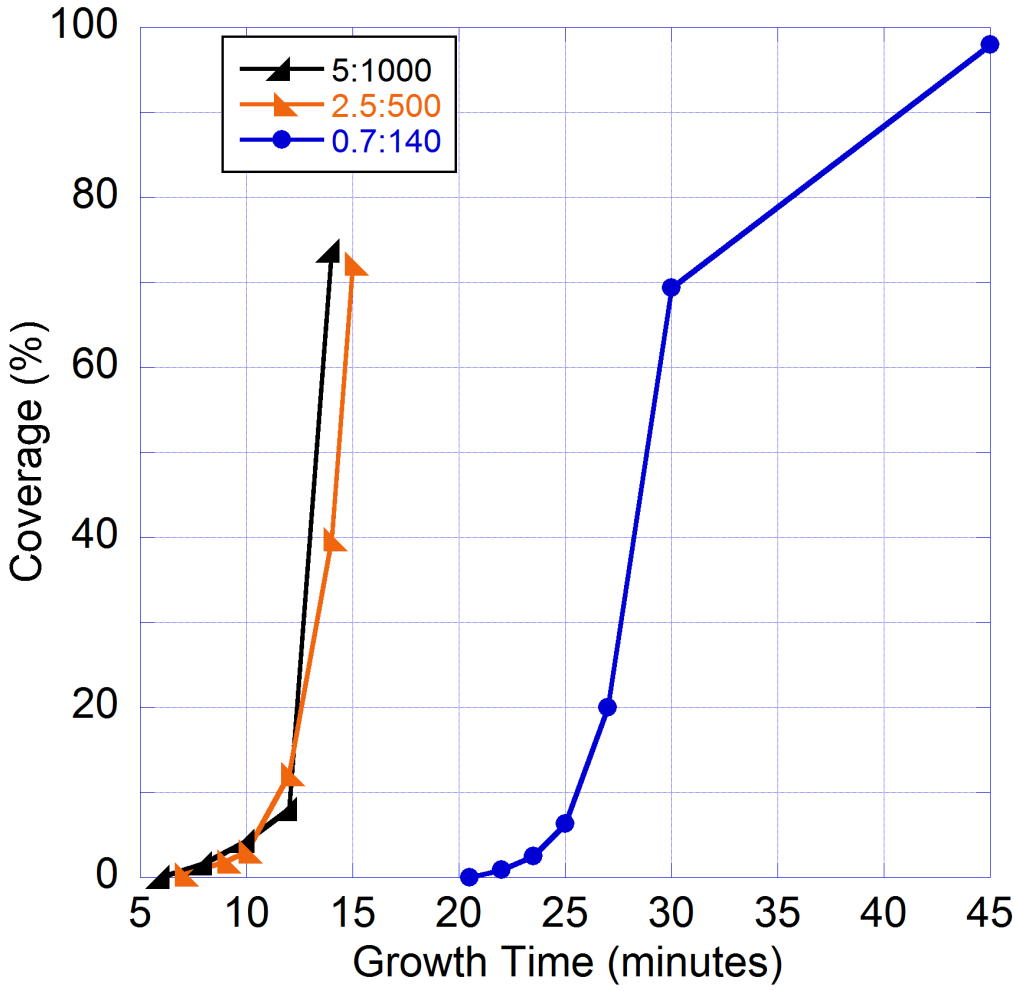

Figure 3. Graphene coverage, θ, vs. growth time for the same samples presented in figure 2. The nucleation time was estimated by linear extrapolation to θ = 0 from the lowest two points of each plot.

Figure 3 plots the graphene coverage, θ, vs. growth time for the same growth conditions as figure 2. Supplementary figure S4 presents a sequence of SEM images showing the graphene morpholgy evolution from the onset of nucleation to completion of a single-layer film for the 0.7:140 plot in figure 3. From these plots, we can estimate the nucleation time, which is the time required for the first graphene crystallites to nucleate, by linear extrapolation to $\theta = 0$ using the lowest 2 points for each growth condition. These nucleation times are 5.8, 6.6 and 20.4 minutes for 5:1000, 2.5:500 and 0.7:140, respectively. These estimated nucleation times are much greater than the ~40 sec required to reach steady-state precursor composition. The nucleation times increase as the Ar dilution increases. This observation reinforces the analogy between CH_4/H_2 dilution with Ar in CVD and deposition rate in PVD discussed above. That is, as the fixed CH_4/H_2 mixture is increasingly diluted with Ar, longer growth times are required to nucleate graphene. In a PVD process, slower deposition rates require longer times for the adatom chemical potential to reach the threshold required to drive nucleation. However, the analogy is imperfect. For PVD the nucleation time scales almost linearly with the inverse of the deposition rate. For the CVD process discussed here, the trend of increasing nucleation time as the Ar dilution increases is analogous to the PVD situation but there does not appear to be a simple scaling relationship between the nucleation time and the Ar dilution. This lack of a simple scaling relationship between nucleation time and Ar dilution of the fixed ratio CH_4/H_2 mixture likely points to the complexity of reaction kinetics in this catalytic system.

Varying the CH_4:H_2 ratio

For this growth series, we quantified the effect of varying the CH_4 : H_2 ratio on graphene film morphology. We varied the H_2 flow rate while keeping all other growth parameters constant. The CH_4 and Ar flow rates were fixed at 0.7 and 10,000 sccm, respectively. The substrate temperature for all growths was 1000°C and the pressure was 700 Torr. We performed 3 runs employing H_2 flows of 140, 280 and 560 sccm. For each of these growth conditions, we grew graphene films for the appropriate times to access the nucleation, growth and impingement and coalescence regimes as graphene coverage increased.

Figure 4(a) plots the average size and nucleation density vs. the growth time for each set of growth parameters. Again, we note that the nucleation density plots for each set of growth parameters can be demarcated into regimes characteristic of a nucleation and growth mechanism. Evident for each set of growth conditions is a nucleation regime, which is the time range for which both the nucleation density and average cluster size increases. Also evident is a growth regime for which N_{sat} has been attained but the average cluster size continues to increase. At N_{sat}, continued deposition eventually results in impingement of the individual grains and their coalescence to form a continuous film. Figure 4(b) summarizes figure 4(a) by plotting N_{sat} and the average graphene cluster size at N_{sat}. Similar to figure 2(b), we also plot $N_{sat}^{-1/2}$ to indicate the average graphene domain size in the continuous single-layer film.

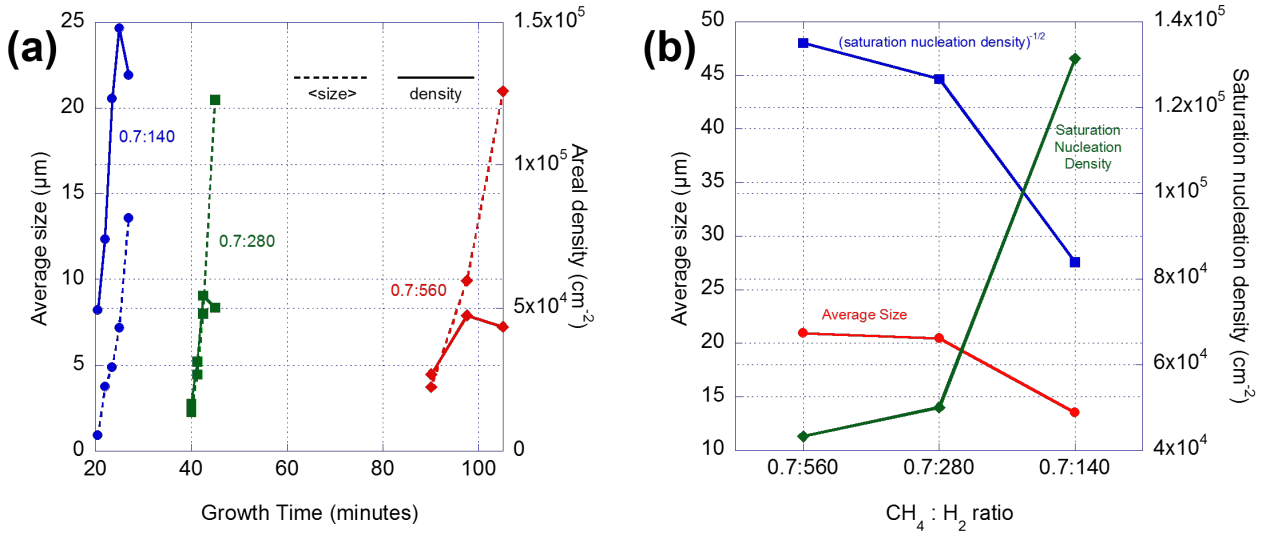

Figure 4. (a) plots average size and nucleation density vs. growth time for graphene crystallites grown at the indicated CH_4 : H_2 flow rates measured in sccm using a total pressure of 700 Torr, a substrate temperature of 1000 °C and an Ar flow rate of 10,000 sccm. (b) summarizes the results of (a), plotting N_{sat} and the average size at the time N_{sat} was reached. It also plots $N_{sat}^{-1/2}$, which measures the average size of graphene grains in a complete single layer graphene film. For the range of growth parameters investigated, a larger range of saturation nucleation densities was attained by varying the CH_4 : H_2 flow ratio than for varying the dilution of a fixed CH_4 : H_2 ratio or by varying the total flow rate.

Figure 5 plots graphene coverage as a function of growth time for the same growth conditions as those plotted in figure 4. As in figure 3, we can estimate the nucleation time by linear extrapolation to $\theta = 0$ using the lowest two data points for each growth condition. We find nucleation times of 20.4, 39.8 and 89.3 minutes for H_2 flow rates of 140, 280 and 560 sccm, respectively. Curiously, these nucleation times scale almost linearly with the H_2 flow rate.

The trend of increased average size and nucleation time and decreased N_{sat} with increasing H_2 flow rate is clear from figures 4 and 5. These observations suggest that increased H_2 partial pressure effectively decreases the C deposition rate and confirm previous findings related to the important role of H_2 in the growth of graphene on Cu from CH_4. It is believed that H_2 can suppress CH_4 decomposition, consequently reducing the C deposition rate on the Cu surface. [39] H_2 also etches existing graphene nuclei during post deposition anneals in H_2/Ar mixtures, as we discuss below. [40] For the 0.7:560 growth series, we observed 1-2μm diameter hexagonal voids etched into the interior of the graphene crystallites for the 120 minute long growth, confirming that the H_2 etching is operative during growth in addition to post-growth annealing.

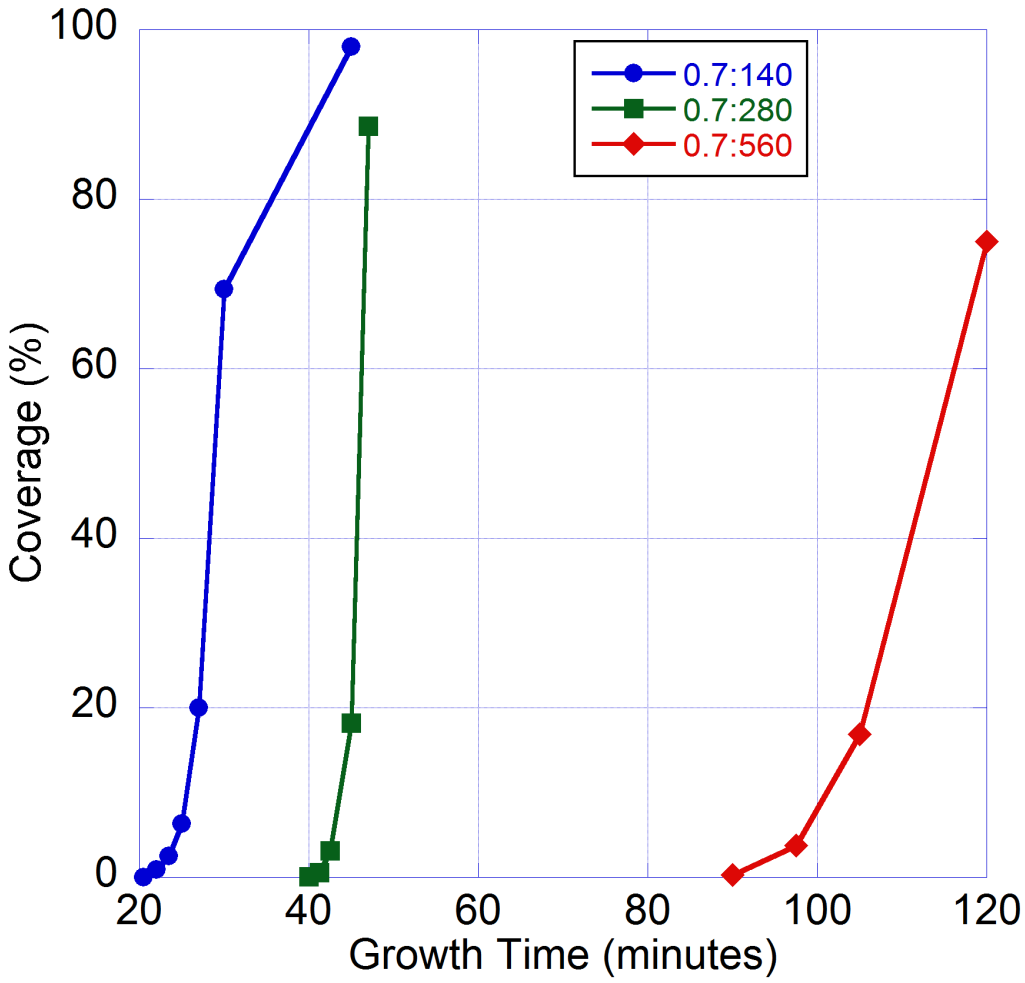

Figure 5. Graphene coverage, θ, vs. growth time for the same samples presented in figure 4. The nucleation time was estimated by linear extrapolation to θ = 0 from the lowest two points of each plot.

Varying the total gas flow rate

We also performed a series of growths to study the effect that varying the total gas flow rate has on graphene film morphology. For this series, we varied the total flow rate while keeping the Ar, H_2 and CH_4 partial pressures the same. To do so, the ratio of the Ar, H_2 and CH_4 flows was kept constant as the total flow was varied. Two different H_2 and CH_4 partial pressures were investigated that corresponded to Ar:H_2:CH_4 flow ratios of 2,000:200:1 or 10,000:200:1. For the first of these flow ratios, the total flow was varied between 550.25 to 11,005 sccm; for the second it was varied from 2,550.25 to 10,201 sccm. For all growths, the total pressure was 700 Torr and the substrate temperature was 1000°C. The results of these experiments are summarized in figure 6.

Figure 6(a) plots the average size and nucleation density vs. the total gas flow rate for both Ar:H_2:CH_4 flow ratios. Within either flow ratio growth run, the graphene films were grown to

nearly identical coverages, as can be seen in figure 6(b). Evidently, as the total flow rate increases, the nucleation density increases and the average size decreases. This behavior is similar to what would be observed for clusters formed via a nucleation and growth mechanism during growth via

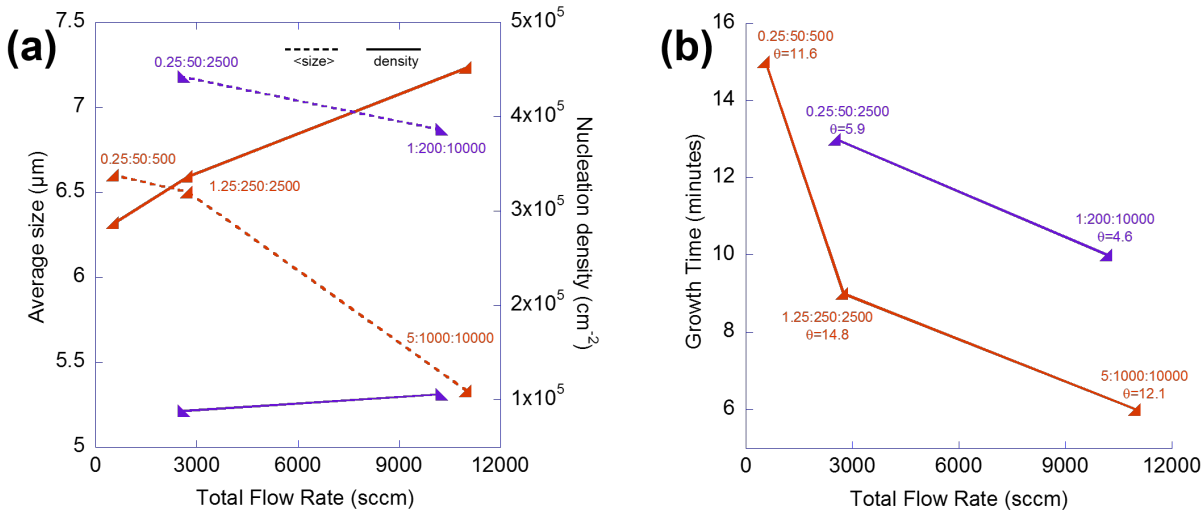

Figure 6. (a) plots the average size and nucleation density of graphene crystallites grown at the indicated CH_4:H_2:Ar flow rates measured in sccm using a total pressure of 700 Torr and a substrate temperature of 1000 °C. If the partial pressure of each precursor is constant while the total flow rate increases, the nucleation density increases and the average size decreases. (b) plots the growth time required to reach nearly identical coverages (indicated near each data point) for each of the flow rates plotted in (a). Evidently, higher flow rates require less time to grow the graphene film to the same coverage. These results indicate that increasing the total flow rate, keeping all other growth parameters the same, is analogous to increasing the deposition rate in a PVD process.

PVD at fixed substrate temperature but different deposition rates. Thus, it appears as if increasing the total gas flow rate while all other growth parameters are fixed in our cold-wall CVD process is analogous to increasing the deposition rate at fixed substrate temperature in a PVD process. This analogy is reinforced by figure 6(b), which plots the growth time required to reach nearly identical graphene coverages vs the total gas flow rate for each of the Ar:H_2:CH_4 flow ratios. The time to reach similar graphene coverages decreases as the total gas flow rate increases. Based on the results shown in figures 6(a) and 6(b) we conclude that increasing the total gas flow rate (keeping all other growth parameters constant) in our cold wall CVD process is analogous to increasing the deposition rate at fixed substrate temperature in a PVD process.

While detailed hydrodynamic modeling of the gas flow in our CVD chamber is beyond the scope of this work, we can gain qualitative insight into the observed behavior by considering stagnation-point flow. Stagnation-point flow describes laminar flow of fluids at normal incidence to an impermeable planar surface (lying in the plane y=0), which is the situation in our vertical flow configuration. 2-D stagnation point flow has a long history in the fluid mechanics literature, beginning with the seminal work of Hiemenz in 1911. [41] Qualitatively, the normally incident

flow transforms into a parallel flow at the substrate surface and the dividing point between streamlines moving along ± x is the stagnation point. Due to the fluid viscosity, the parallel flow velocity is reduced to zero along the fluid/solid boundary and achieves 99% of its free-stream value at the boundary layer thickness, δ.

Since the normal flow converts to a parallel flow at the surface, the boundary layer thickness can reasonably be approximated by the Blasius solution, which describes flow parallel to a flat plate, $\delta = 5\sqrt{(\nu L/U)}$.[42] ν is the kinematic viscosity, L is a characteristic length related to the system geometry and U is the free stream parallel velocity (*i.e.*, the parallel velocity just outside the boundary layer). Since U should scale linearly with the total gas flow rate, the boundary layer is thicker at low total flow and thinner at high total flow. As a consequence, reactants depleted at the substrate surface require a longer time to be replenished by diffusion through the thicker boundary layer at low flow rates. An additional effect may also conspire to produce the behavior evident in figure 6. The stagnation pressure is higher than the pressure far from the surface. [43] However the pressure gradient normal to the surface is of order $\nu^{1/2}$, which will be negligible for the low viscosity fluids under consideration.

Graphene nucleus shape and crystallinity

In addition to the variations in graphene nucleation density and growth rates discussed above, we also observed that the graphene nucleus shape was growth parameter dependent. First, we note that more-or-less hexagonal graphene nuclei were a single crystal. In contrast, non-hexagonal crystallites were polycrystalline. Hexagonal graphene nuclei were bound by six sides. While side morphology depended on growth conditions as discussed below, adjacent sides were oriented with an average angle of 120° between them. Most non-hexagonal graphene crystallites were polygonal and bound by more than 6 sides. The adjacent sides of these polygonal crystallites were oriented at angles that differ from 120°. A relatively small fraction of the non-hexagonal crystallites had irregular boundaries. Whether or not these graphene nuclei were single- or polycrystalline could be revealed using the post-growth H-etching method of Guo, et. al. [40]

Examples of etched single and bi-crystalline graphene nuclei are shown in figure 7. Subsequent to growth using 0.7:280:10000 sccm of CH_4:H_2:Ar at a total pressure of 700 Torr and substrate temperature of 1000°C for 45 min, the CH_4 flux was terminated. The sample was annealed at 1000°C for an additional 10 minutes in 280:10000 sccm of H_2:Ar at 700 Torr. This additional H_2 annealing step resulted in the etched hexagonal voids apparent in the interior of the graphene nuclei. Since H_2 etching preferentially exposes zig zag edges, [28, 39, 44] the orientation of these etched hexagons reveals the crystalline nature of the graphene nucleus and enables the misorientation between the single crystal grains of a polycrystalline nucleus to be identified.

Figure 7(a) displays a hexagonal graphene crystallite with three well-developed etched hexagonal voids apparent in its interior. These etched hexagons are oriented parallel to each other and to the edges of the parent graphene crystallite, indicating that it is a single crystal. In contrast, figure 7(b) displays a non-hexagonal graphene crystallite with several features etched in its interior. Those highlighted in white are misoriented by about 20° relative to those highlighted in black. This polygonal crystallite is likely the result of two merged single crystal hexagons. The two crystallites

resulted from separate nucleation events and eventually impinged to form a single, polygonal crystallite. This interpretation is supported by the observation that the incidence of non-hexagonal graphene crystallites increases as the graphene coverage increases. The following discussion of graphene crystallite shape is restricted to those that can be conclusively identified as single crystals that resulted from an isolated nucleation event.

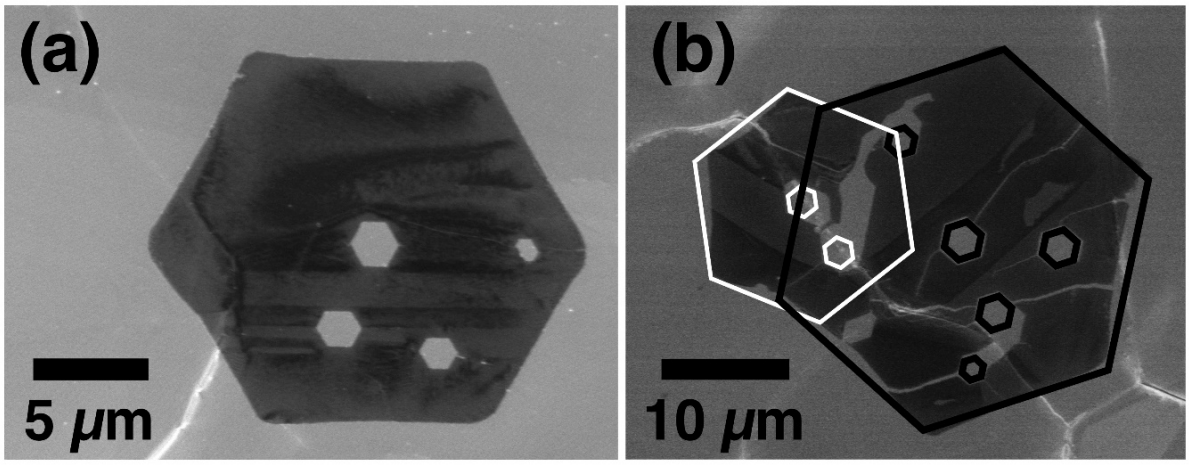

Figure 7. SEM images of (a) a single crystal and (b) a bi-crystalline graphene nucleus from the same sample grown for 45 minutes at a substrate temperature of 1000°C, total pressure of 700 Torr and Ar, H_2 and CH_4 flow rates of 10,000, 280 and 0.7 sccm, respectively. Subsequent to growth, the sample was annealed in the Ar and H_2 ambient at the growth temperature for 10 mins producing the interior voids. In (a) the hexagonal voids are crystallographically aligned to each other and to the edges of the parent crystallite. In (b) the white (black) highlighted voids are oriented parallel to each other and to the white (black) highlighted graphene crystallite. During growth, these two crystallites merged to form the bicrystal.

Figure 8 summarizes the evolution of graphene crystallite shape with growth conditions. Figures 8(a)-8(c) were all grown at a CH_4:H_2 ratio = 1:200 but with increasing Ar dilution. As a consequence, the effective C deposition rate decreases from figure 8(a) to 8(c). Figures 8(d) and (e) were grown at lower CH_4:H_2 ratios of 1:400 and 1:800, respectively. So their growth rates are smaller than the sample depicted in figure 8(c) and the growth rate of the sample shown in figure 8(e) is slower than the sample shown in figure 8(d).

We identify three distinct graphene crystallite shapes. The first is bound by irregular, jagged edges. An example of this crystallite shape is arrowed in figure 8(a). The second distinct shape is a convex hexagon. These crystallites are hexagonal but are bound with convex instead of straight edges; an example is arrowed in figure 8(b). The third crystallite shape is a regular hexagon; an example is arrowed in figure 8(c). Note that crystallites bound by irregular edges are found only at the highest growth rates, in figures 8(a) and 8(b). As the growth rate continues to decrease from figures 8(b) to 8(e), the graphene crystallite morphology progresses from convex hexagons to regular hexagons. To summarize, at the highest effective C deposition rates, some of the graphene crystallites are

bound by irregular, jagged edges. At lower deposition rates, the crystallites grow as convex hexagons and at the lowest deposition rates the crystallites are regular hexagons bound by straight edges.

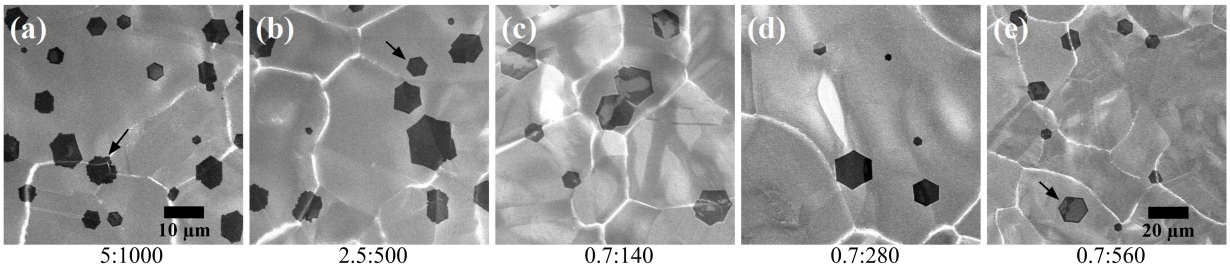

Figure 8. SEM images of samples grown at 700 Torr and a substrate temperature of 1000°C. The Ar flow rate was 10,000 sccm and the CH_4:H_2 flows are indicated below each image. (a)-(e) were grown for 12, 12, 25, 42.5 and 97.5 minutes, respectively. In (a), a crystallite with an irregular, jagged boundary is arrowed. In (b) a convex hexagonal crystallite is arrowed. In (e) a hexagonal crystallite is arrowed. This sequence of images depicts the progression of graphene crystallite morphology as the growth rate decreases from (a) to (e). The scale bar is the same for (a)-(d).

Similar behavior was observed for growth via hot wall CVD by Vlassiouk, *et al*. [28] A quantitative comparison to our results is challenging due to the difference in growth methods and since they employed a much lower total flow rate of 500 sccm compared to the 10,000 sccm employed here. However, they did observe the same sequence of graphene crystallite edge morphologies as those presented here. As the CH_4:H_2 flow ratios decreased, the graphene crystallites were bound by edges that progressed from irregular/jagged to convex (star-shaped) to straight (regular hexagons). They attributed this behavior to a variation in the balance between H_2 etching of the graphene crystallite edges and C-incorporation at their perimeter. At higher H_2 flows, etching more effectively exposes zig zag edges leading to regular hexagonal crystallites with straight edges. In contrast, at lower H_2 flows etching is suppressed leading to an irregular, jagged morphology.

H_2 etching is certainly important during graphene growth, as evidenced by the appearance of hexagonal voids within graphene crystallites grown using 0.7:560 CH_4:H_2 ratio discussed previously. However, it is likely that the relative rates of C adatom arrival from the substrate and C diffusion along the edges of graphene crystallites are also important. If the edge diffusion rate is not rapid enough, C atoms can be kinetically trapped by arriving C adatoms, leading to roughened graphene edges. [45,46] Simple modeling by Vlassiouk, *et al*. suggested that the vertices of hexagonal graphene crystallites incorporated C more rapidly by virtue of a larger concentration gradient than the edge center. [28] With a sufficient edge diffusion rate, the star-shaped, convex hexagonal morphology predicted by their model would not develop. Further work is required to conclusively identify the contributions of H-etching and edge diffusion to graphene crystallite morphology. However, our observation that the progression of edge morphology from irregular/jagged to convex and finally to straight occurs as the effective C deposition rate decreases suggests that the relative rates of C adatom incorporation and edge diffusion play a role in crystallite morphology.

4. CONCLUSION

The nucleation density and average size of graphene crystallites grown on electrodeposited Cu films using cold wall CVD from Ar, H_2 and CH_4 mixtures can be tuned by varying the growth parameters. For growth at a fixed substrate temperature of 1000°C and total pressure of 700 Torr, decreasing the CH_4:H_2 ratio, decreasing the concentration of the CH_4+H_2 mixture at fixed CH_4:H_2 ratio and decreasing the total flow rate all decreased the growth rate of the graphene film. This decrease in growth rate leads to smaller nucleation densities and larger average nucleus size. For the range of growth conditions investigated, the largest variation of the nucleation density was obtained by varying the CH_4:H_2 ratio.

For all conditions investigated, graphene grows via a nucleation and growth mechanism. At the smallest deposition times, the chemical potential of diffusing C-containing species is not large enough to drive nucleation and no graphene crystallites were observed. Subsequent to nucleation of the first graphene crystallites, the nucleation density increases while existing nuclei grow during the nucleation phase. Upon reaching the saturation nucleation density, the C chemical potential stabilizes at a value below that required to drive additional nucleation since all additional C resulting from CH_4 decomposition can diffuse to existing crystallites. Continued growth results in eventual impingement of the isolated crystallites and formation of a single-layer polycrystalline graphene film.

We also found that the boundary morphology of graphene crystallites depends on growth conditions; progressing from irregular/jagged through convex hexagonal to regular hexagonal as the effective C deposition rate increases. This observation suggests that, in addition to H_2 etching, C adatom diffusion along the edge of growing graphene crystallites may play an important role in the morphology evolution of graphene nuclei.

These results conclusively determine that the growth mode of graphene using cold wall CVD is similar to that of hot wall CVD. Both follow a nucleation and growth mechanism, suggesting that the large hot wall CVD knowledge base may be extrapolated to the industrially relevant cold wall CVD method.

AUTHOR INFORMATION

*Email: jeff.drucker@asu.edu

ACKNOWLEDGMENTS

This work was supported by the National Science Foundation (DMR-1409280).

References

(1) Novoselov, K. S.; Geim, A. K.; Morozov, S. V.; Jiang, D.; Zhang, Y.; Dubonos, S. V.; Grigorieva, I. V.; Firsov, A. A. Electric Field Effect in Atomically Thin Carbon Films. *Science* **2004**, 306, 666–669.

(2) Garlow, J. A.; Barrett, L. K.; Wu, L.; Kisslinger, K.; Zhu, Y.; Pulecio, J. F. Large-Area Growth of Turbostratic Graphene on Ni (111) via Physical Vapor Deposition. *Scientific Reports* **2016**, 6, 19804.

(3) Mua, W.; Fu, Y.; Sun, S.; Edwards, M.; Ye, L.; Jeppson, K.; Liu, J. Controllable and fast synthesis of bilayer graphene by chemical vapor deposition on copper foil using a cold wall reactor. *Chem. Engg. Journal* **2016**, 304, 106–114

(4) Wu, C.; Li, F.; Chen, W.; Veeramalai, C. P.; Ooi, P. C.; Guo, T. Electromagnetic induction heating for single crystal graphene growth: morphology control by rapid heating and quenching. *Scientific Reports* **2015**, 5, 9034.

(5) Reina, A.; Jia, X.; Ho, J.; Nezich, D.; Son H.; Bulovic V.; Dresselhaus, M.S.; Kong, J. Large Area Few Layer Graphene Films on Arbitrary Substrates. *Nano Lett.*, **2009**, 9 (1), 30-35.

(6) Wu, W.; Jauregui, L. A.; Su, Z.; Liu, Z.; Bao, J.; Chen, Y. P.; Yu, Q. K. Growth of Single Crystal Graphene Arrays by Locally Controlling Nucleation on Polycrystalline Cu Using Chemical Vapor Deposition. *Adv. Mater.* **2011**, 23, 4898–4903.

(7) Robertson, A.W.; Warner, J.H. Hexagonal Single Crystal Domains of Few-Layer Graphene on Copper Foils. *Nano Lett.,* **2011**, 11, 1182–1189.

(8) Li, X. S.; Magnuson, C. W.; Venugopal, A.; Tromp, R. M.; Hannon, J. B.; Vogel, E. M.; Colombo, L.; Ruoff, R. S. Large-Area Graphene Single Crystals Grown by Low-Pressure Chemical Vapor Deposition of Methane on Copper. *J. Am.Chem. Soc.* **2011**, 133, 2816–2819.

(9) Wu, B.; Geng, D.; Guo, Y.; Huang, L.; Xue, Y.; Zheng, J.; Chen,J.; Yu, G.; Liu, Y.; Hu, W. Equiangular Hexagon-Shape-Controlled Synthesis of Graphene on Copper Surface. *Adv. Mater.* **2011**, 23, 3522–3525.

(10) Yu, Q. K.; Jauregui, L. A.; Wu, W.; Colby, R.; Tian, J.; Su, Z.; Cao, H.; Liu, Z.; Pandey, D.; Wei, D. Control and Characterization of Individual Grains and Boundaries in Graphene Grown by Chemical Vapor Deposition. *Nat. Mater.* **2011**, 10, 443–449.

(11) Li, X. S.; Cai, W. W.; An, J. H.; Kim, S.; Nah, J.; Yang, D. X.; Piner,R.; Velamakanni, A.; Jung, I.; Tutuc, E.; Banerjee, S.K.; Colombo, L; Ruoff, R.S. Large-Area Synthesis of High-Quality and Uniform Graphene Films on Copper Foils. *Science* **2009**, 324, 1312–1314.

(12) Wu, Y.A.; Fan, Y; Speller, S; Creeth, G.L.; Sadowski, J.T.; He, K.; Robertson, A.W.; Allen, C.S.; Warner, J.H. Large Single Crystals of Graphene on Melted Copper Using Chemical Vapor Deposition. *ACS Nano*, **2012**, 6(6), 5010-5017.

(13) Mattevi, C.; Kima, H.; Chhowalla, M. A review of chemical vapor deposition of graphene on copper. *J. Mater. Chem.*, **2011**, 21, 3324–3334.

(14) Li, Z.; Wu, P.; Wang, C.; Fan, X.; Zhang, W.; Zhai, X.; Zeng, C.; Li, Z.; Yang, J.; Hou, J. Low-Temperature Growth of Graphene by Chemical Vapor Deposition Using Solid and Liquid Carbon Sources. *ACS Nano* **2011**, 5(4), 3385-3390.

(15) Kidambi P.R.; Ducati C.; Dlubak B.; Gardiner D.; Weatherup R.S.; Martin MB.; Seneor P.; Harry Coles H.; Hofmann S. The Parameter Space of Graphene Chemical Vapor Deposition on Polycrystalline Cu. *J. Phys. Chem. C* **2012**, 116, 22492–22501.
(16) Luo, Z.; Kim, S.; Kawamoto, N.; Rappe, A. M.; Johnson, A. T. C. Growth Mechanism of Hexagonal-Shape Graphene Flakes with Zigzag Edges. *ACS Nano* **2011**, 5, 9154–9160.
(17) Wang, H.; Wang, G.; Bao, P.; Yang, S.; Zhu, W.; Xie, X.; Zhang, W.-J. Controllable Synthesis of Submillimeter Single-Crystal Monolayer Graphene Domains on Copper Foils by Suppressing Nucleation. *J. Am. Chem. Soc.* **2012**, 134, 3627–3630.
(18) Gao, L.; Ren, W.; Zhao, J.; Ma, L.-P.; Chen, Z; Cheng, H.-M. Efficient Growth of High-quality Graphene Films on Cu Foils by Ambient Pressure Chemical Vapor Deposition. *Appl. Phys. Lett.* **2010**, 97, 183109.
(19) Bhaviripudi, S.; Jia, X.; Dresselhaus, M. S.; Kong, J. Role of Kinetic Factors in Chemical Vapor Deposition Synthesis of Uniform Large Area Graphene Using Copper Catalyst. *Nano Lett.* **2010**, 10 (10), 4128–4133.
(20) Wu, B.; Geng, D.; Xu, Z; Guo, Y.; Huang, L.; Xue, Y.; Chen, J.; Yu, G.; Liu, Y. Self-organized graphene crystal patterns. *NPG Asia Materials*, **2013**, 5, e36.
(21) Vlassiouk, I.; Fulvio, P.; Meyer, H.; Lavrik, N.; Dai, S.; Datskos, P.; Smirnov, S. Large scale atmospheric pressure chemical vapor deposition of graphene. *Carbon*, **2013**, 54, 58-67.
(22) Zhou, H.; Yu, W. J.; Liu, L.; Cheng, R.; Chen, Y.; Huang, X.; Liu, Y.; Wang, Y.; Huang, Y.; Duan, X. Chemical vapour deposition growth of large single crystals of monolayer and bilayer graphene. *Nat Commun*, **2013**, 4.
(23) Lee, Y.; Bae, S.; Jang, H.; S. Jang, S.-E. Zhu, S. H. Sim, Y. I. Song, B. H. Hong and J.-H. Ahn Wafer-Scale Synthesis and Transfer of Graphene Films *Nano Lett.* **2010**, 10, 490-493.
(24) Bae, S.; Kim, H.; Lee, Y.; Xu, X. F.; Park, J. S.; Zheng, Y.; Balakrishnan, J.; Lei, T.; Kim, H. R.; Song, Y. I. Roll-to-Roll Production of 30-inch Graphene Films for Transparent Electrodes. *Nat. Nanotechnol.* **2010**, 5, 574–578.
(25) Bointon T.H.; Barnes M.D.; Russo S.; Craciun M.F. High Quality Monolayer Graphene Synthesized by Resistive Heating Cold Wall Chemical Vapor Deposition *Adv. Mater.* **2015**, 27, 4200–4206
(26) Miseikis V.; Convertino D.; Mishra N.; Gemmi M.; Mashoff T.; Heun S.; Haghighian N.; Bisio F.; Canepa M.; Piazza V.; Coletti C. Rapid CVD growth of millimetre-sized single crystal graphene using a cold-wall reactor *2D Materials*, **2015**, 2(1), 014006
(27) Wang Z.J.; Weinberg G.; Zhang Q.; Lunkenbein T.; Klein-Hoffmann A.; Kurnatowska M.; Plodinec M.; Li Q.; Chi L.; Schlögl R.; Willinger MG. Direct Observation of Graphene Growth and Associated Copper Substrate Dynamics by in Situ Scanning Electron Microscopy *ACS Nano* **2015**, 9(2), 1506-1519.
(28) Vlassiouk, I.; Smirnov, S.; Surwade, S.P.; Regmi M.; Srivastava, N.; Feenstra, R.; Eres, G.; Parish, C.; Lavrik, N., Datskos, P.; Dai, S.; Fulvio, P. Graphene Nucleation Density on Copper: Fundamental Role of Background Pressure. *J. Phys. Chem. C* **2013**, 117 (37), 18919–18926.
(29) Xing, S.; Wu, W.; Wang Y.; Bao J.; Pei SS. Kinetic study of graphene growth: Temperature perspective on growth rate and film thickness by chemical vapor deposition. *Chem. Phys. Lett.* **2013**, 580, 62–66.

(30) Fromm, E. Reduction of metal evaporation losses by inert gas atmospheres. *Met. Trans. A,* **1978** 9(12), 1835-1838.
(31) Rasband, W.S., ImageJ, U. S. National Institutes of Health, Bethesda, Maryland, USA, **1997-2016**; http://imagej.nih.gov/ij/ .
(32) Ferrari, A. C.; Meyer, J. C.; Scardaci, V.; Casiraghi, C.; Lazzeri, M.; Mauri, F.; Piscanec, S.; Jiang, D.; Novoselov, K. S.; Roth, S.; Geim, A. K. Raman spectrum of graphene and graphene layers. *Phys. Rev. Lett.* **2006**, 97, No. 187401.
(33) Ferrari, A. C. and D. M. Basko Raman spectroscopy as a versatile tool for studying the properties of graphene. *Nat Nano,* **2013**, 8(4), 235-246.
(34) Costa, S.D.; Righi, A.; Fantini C.; Hao, Y.; Magnuson, C.; Colombo, L.; Ruoff, R.S.; Pimenta, M.A. Resonant Raman spectroscopy of graphene grown on copper substrate *Solid State Comm.* **2012**, 152, 1317–1320.
(35) Yin, X.; Li, Y.; Lin, F.K.C.; Zhao, H.; Gan L.; Luo Z.; Zhao, R.; Heinz T.F.; Hu, Z. Evolution of the Raman spectrum of graphene grown on copper upon oxidation of the substrate. *Nano Research* **2014**, 7(11), 1613–1622.
(36) Wood, J.D.; Schmucker, S.W.; Lyons, A.S.; Pop, E.; Lyding, J.W. Effects of Polycrystalline Cu Substrate on Graphene Growth by Chemical Vapor Deposition *Nano Lett.* **2011**, 11, 4547–4554.
(37) Stroscio, J.A.; Pierce, D.T. Scaling of diffusion-mediated island growth in iron-on-iron homoepitaxy. *Phys. Rev. B* **1994**, 49, 8522-8525.
(38) Ratsch C.; Zangwill, A; Smilauer, P; Vvedensky, D.D. Saturation and scaling of epitaxial island densities, *Phys. Rev. Lett.* **1994**, 72, 3194-3197
(39) Vlassiouk I.; Regmi M.; Fulvio P.; Dai S.; Datskos P.; Eres G.; Smirnov S. Role of Hydrogen in Chemical Vapor Deposition Growth of Large Single-Crystal Graphene *ACS Nano* **2011**, 5(7), 6069-6076.
(40) Guo, W.; Wu, B.; Li, Y.; Wang, L.; Chen, J.; Chen, B.; Zhang, Z.; Peng, L.; Wang, S.; Liu, Y. Governing Rule for Dynamic Formation of Grain Boundaries in Grown Graphene. *ACS Nano* **2015**, 9(6), 5792-5798.
(41) Hiemenz K. Die Grenzschicht an einem in den gleichformigen flussigkeitsstrom eingetauchten geraden kreiszylinder. *Dinglers Polytech. J.* **1911**, 326, 321.
(42) Blasius H. Grenzschichten in flussigkeiten mit kleiner reibung. *Z. Angew Math. Phys.* **1908**, 56, 1.
(43) Schlichting H.; Gersten K. *Boundary Layer Theory*; Springer-Verlag Berlin Heidelberg, **2000**, 112.
(44) Guo, Y.; Guo, W. Favorable Zigzag Configuration at Etched Graphene Edges. *J. Phys. Chem. C* **2011**, 115, 20546–20549.
(45) Geng D.; Meng L.; Chen B.; Gao E.; Yan W.; Yan H; Luo B.; Xu J.; Wang H.; Mao Z.; Xu Z.; He L.; Zhang Z.; Peng L.; Yu G. Controlled Growth of Single-Crystal Twelve-Pointed Graphene Grains on a Liquid Cu Surface, *Adv. Mater.* **2014**, 26, 6423.
(46) Artyukhov V.I.; Liu Y.; Yakobson B.I. Equilibrium at the edge and atomistic mechanisms of graphene growth *PNAS,* **2012**, 109 (38), 15136-15140.